Improvement of Formability and Corrosion Resistance of Az31 Magnesium Alloy by Pulsed Current-assisted Laser Shock Forming

Huixia Liu (lhx@ujs.edu.cn)
Jiangsu University
Yuhao Sun
Jiangsu University
Youjuan Ma
Jiangsu University
Yanchen He
Jiangsu University
Xiao Wang
Jiangsu University

Research Article

Keywords: Formability, Corrosion, Pulse current, Laser shock forming

Posted Date: April 7th, 2021

DOI: https://doi.org/10.21203/rs.3.rs-372938/v1

Version of Record: A version of this preprint was published at The International Journal of Advanced Manufacturing Technology on April 13th, 2022. See the published version at https://doi.org/10.1007/s00170-022-09211-2.

Abstract

This study adopted a novel pulse current-assisted laser shock AZ31B sheet micro-forming method (EP-LSF). The mechanism of improving the formability of AZ31B Magnesium Alloy by pulse current assisted laser shock forming and the reason of improving the corrosion resistance were studied for the first time. Through laser shock free bulging experiment, tensile test, optical microscope (OM), and X-ray diffraction, the change in formability was studied. After pulse current assisted laser shock forming, the forming height of AZ31B magnesium alloy increases by 28.8%, the thinning rate decreases by 6.7%, and the strain rate sensitivity coefficient increases to 0.1452. The results show that the decrease of grain size and texture density is the reason why EP-LSF can further improve the formability of AZ31B magnesium alloy. The changes in corrosion resistance were studied by scanning electron microscopy and electrochemical tests. The results show that after EP-LSF, the corrosion current density of AZ31 magnesium alloy decreased, and the electrochemical impedance increased, indicating that this method further improved the corrosion resistance.

Introduction

In recent years, lightweight and miniaturized parts have become an unstoppable global trend in many industrial fields and have been widely used in biomedicine, electronic appliances, aerospace, and other fields. Magnesium alloys meet the requirements of lightweight materials due to their low density, high specific strength and rigidity, excellent machining performance, and good damping and shock absorption properties [1,2]. However, due to their densely packed hexagonal crystal lattice structure, and poor plasticity, magnesium alloys are active and easy to corrode [3–6], thereby limiting their application in micro-parts. Therefore, a high-efficiency microplastic forming technology that can improve the plasticity and corrosion resistance of magnesium alloys must be adopted.

Laser shock micro-forming (LSF) technology is a new technology that has developed rapidly in recent years. This, technology has been widely used in research fields, such as material forming, because it does not require the production of high-precision micro-punch molds [7], reduces size effects [8], and improves the material forming performance [9]. At present, more laser shock forming studies have been conducted on copper, stainless steel, and other materials [7–9] than on lightweight materials, such as magnesium alloys, and the forming ability of materials with poor plasticity (e.g., magnesium, aluminum, and titanium alloys) and complex micro characteristics is still insufficient.

In recent years, the improvement of the forming properties of magnesium alloys has gradually attracted the attention of many researchers. Liu et al. [10] observed the presence of electro-plasticity in AZ31 magnesium alloy through tensile tests and found that pulse current increased the elongation and reduced the flow stress of the sample. Feng et al. [11] found through tensile test research that high strain rate can increase the elongation of magnesium alloy. Studies have shown that grain refinement can effectively improve the forming properties of materials [12]. Song et al. [13] used high-density electric pulses to treat as-cast Ti-Al alloys and found that electric pulse treatment is an effective method of refining the grains of

titanium alloys. Xu [14] found that high strain rate can refine the processed surface grain, indicating that electric pulse and high strain rate can improve the forming ability by refining the grain. The strength of the texture also affects the forming performance of materials. That is, the lower the texture density is, the better the forming ability of the material will be [15]. Jiang et al. [16] used X-ray diffraction (XRD) and electron backscatter diffraction to study the effect of electric pulse treatment on the texture evolution of AZ91 magnesium alloy and found that electric pulse treatment advantageously weakens the strength of the basic texture of the magnesium alloy. Tiwari et al. [17] used a split Hopkinson torsion bar (SHTB) to study the deformation behavior of aluminum-zinc-magnesium-copper alloys at high strain rates and found that the overall texture of the alloy weakened as the strain rate increased. This shows that electric pulse and high strain rate can reduce the texture density to improve the forming ability.

The improvement of the corrosion resistance of magnesium alloys is also a popular research topic. Liu [18] processed magnesium-4Sm alloy using high-current pulsed electron beam, tested the corrosion of the sample through electrochemical test, and found that the corrosion current density decreased, the electrochemical impedance increased, and the corrosion resistance improved. M. Abeens [19] found that the sample grains treated by laser shot peening were refined, the grain boundary density increased, the crack propagation was delayed, and the corrosion rate was effectively reduced. Caralapatti et al. [20] studied the effect of laser shock repetition rate on the corrosion resistance of magnesium alloys and found that the overlap percentage has a major impact on the corrosion rate. The corrosion rate decreases as the overlap increases, indicating that electrical pulses and high strain rates can improve the corrosion resistance of materials.

According to the above research, pulse current and high strain rate treatment are beneficial to improving magnesium alloy formability and corrosion resistance. LSF is a high strain rate forming technology suitable for micro forming. In this paper, combining the advantages of pulse current and LSF, a method based on pulse current-assisted laser shock AZ31 magnesium alloy foil micro forming is proposed to solve the problems with magnesium alloy properties, namely, difficult to form and easy to corrode. Theoretical and experimental analyses reveal the forming mechanism of laser shock foil micro-forming based on electro-plasticity and the mechanism of pulse current-assisted laser shock to improve the corrosion resistance of materials.

Experiments

2.1 Materials

This study used AZ31 magnesium alloy. The size of the forming experiment sample was 10 mm × 10 mm × 0.1 mm, and the electrochemical experiment sample size was 10 mm × 10 mm × 0.5 mm. The surface of the sample was washed with absolute ethanol before the experiment. The chemical composition of the AZ31 magnesium alloy is listed in Table 1.

Table 1 Chemical Composition (wt.%) of AZ31.

Al	Zn	Mn	Fe	Si	Cu	Ni	Mg
2.75	0.64	0.27	0.0023	0.018	0.0016	0.00055	Balance

2.2 Pulse current processing

The experiment used a CTNP1621-30/4000FN pulse current generator to pre-process the sample. The experimental parameters of the pulse current generator in the experiment were as follows: voltage, 10 V; frequency, 50 Hz; root mean square current, 25 A. The peak pulse current was set to 25, 30, and 35 A by changing the duty cycle value, and the pulse current duration was 60 s. Before applying pulse current, the surface of the sample was sprayed with lra-15 boron nitride anti-oxidation coating to prevent the surface oxidation of the sample. The two ends of the sample were connected with a copper electrode after chromium plating treatment. The temperature distribution on the surface of the sample was measured and recorded by a GIS10000C infrared thermometer. After the pretreatment, the boron nitride anti-oxidation coating on the surface of the sample was removed with absolute ethanol, and the remaining liquid and impurities on the surface of the sample were cleaned with pure water for the subsequent experiments.

2.3 Micro-bulging experiment under laser shock loading

To test the micro-forming properties of the cold-rolled and pulse current treated samples under high strain rate loading, A Spitlight 2000 Nd: YAG laser was used in the experiment. The maximum energy of the pulse laser was 1.4 J. The diameter of the spot was 2.5 mm. The experiment was divided into three groups: cold rolling, 25- and 30-A pulse current treatment, and then each group was impacted by 40% laser energy. A KEYENCE VHX-1000C microscope was used to observe and characterize the forming height and thinning rate. Figs. 1(a) and (b) present the experimental schematics and die diagram of EP-LSF, respectively.

2.4 Tensile tests

To investigate the effect of pulse current on the strain rate sensitivity coefficient of magnesium alloy, a UTM4104 microcomputer-controlled electronic universal testing machine was used in the tensile experiment. Before the experiment, the pre-processed material was cut into the sample shown in Fig. 2 by electric spark cutting according to ASTM E345. The equal strain rate stretching method was used to determine the strain rate sensitivity coefficient, and five different levels of strain rate were set, namely, 0.5, 1, 2, 5, and 10 mm/min, for stretching. The σ–ε curve was obtained.

2.5 Microstructure characterization

To investigate the microstructure of magnesium alloys after EP-LSF, various characterization techniques were used.

2.5.1 OM

To study the effect of EP-LSF on the grain size of AZ31 magnesium alloy, the samples were polished sequentially with 400# to 3000# sandpapers and mechanically polished with a 0.5-μm diamond polishing agent. The corrosion solution was made of 1 ml of nitric acid, 20 ml of acetic acid, 60 ml of ethylene glycol, and 19 mL of water. After corrosion, the sample was placed in water-free ethanol, cleaned using an ultrasonic cleaning machine for

300 s, and dried using an air cooler. Then, a DMI8A metallurgical microscope was used to observe the cross-sectional crystal grains of the sample.

2.5.2 Macro texture

To study the effect of EP-LSF on texture density of AZ31 magnesium alloy, the texture distribution of AZ31 magnesium alloy was observed by RIGAKU X-ray diffractometer. The scanning angle ranged from 30°-90°, and the scanning rate was 5°/min.

2.5.3 X-ray diffraction

In the XRD test, BRUKER D8 ADVANCE X-ray diffractometer was used, the scanning angle ranged from 10° to 90°, and the scanning rate was 5°/min. Then, phase analysis was performed on the magnesium alloy.

2.6 Corrosion resistance

2.6.1 Scanning electron microscopy

To study the effect of EP-LSF on the corrosion resistance of magnesium alloys, the experiment was divided into four groups: the cold rolled state, the 80% laser energy impact sample, the 35-A pulse current treatment, and the 35-A pulse treatment after 80% laser energy impact. The treated sample was corroded in 3.5% NaCl solution for 1 h, the residual liquid on the sample surface was washed with pure water and dried, and then the corrosion morphology of the sample surface was observed with a S-3400N scanning electron microscope.

2.6.2 Electrochemical measurements

In the experiment, a Princeton versastat 4 electrochemical work-station was used to determine the polarization curve and for electrochemical impedance spectroscopy (EIS). The specimen was welded with copper wire, and the non-working surface was sealed with epoxy resin. A three-electrode system was adopted, the auxiliary electrode was graphite electrode, the reference electrode was saturated calomel electrode, and the electrolyte was 3.5% NaCl solution. The experiment was performed at room temperature. The constant potential scanning method was used, and the scan rate was 5 mV/s. The standing time was 300 s, the measuring potential range was -3−2.5 V, the scanning speed was 1 mV/s, the termination potential was 0 V, and the electrochemical impedance test frequency range was 0.5−10 kHz.

Results And Discussion

3.1 Surface morphology

3.1.1 Forming height

Fig. 3 (a) shows the cold-rolled sample. Figs. 3(b) and (c) show the 25-and 30-A pulse current treatment samples, respectively. The measurement results of the forming height in Section 2.3 of the experiment are shown in Fig. 4. The average forming height of the cold-rolled state is 193.7 μm. the average forming height is 238.42 μm, when 25-A current is applied, and the forming height is increased by 23.1%. the average forming height is 249.4

μm, When 30-A current is applied, showing an increase of 28.8%. The experimental results show that the forming height of the material increases significantly as the current density increases, indicating that EP-LSF can effectively improve the micro-forming ability of magnesium alloys.

3.1.2 Thinning rate

The experiment was divided into two groups: the cold-rolled state and the 30-A pulse current treatment, which were impacted by 40% laser energy. After laser shock forming, the thickness in the forming area decreased, and the thickness reduction varied at different positions. The closer to the top of the forming area was, the greater the thinning rate was. Therefore, seven positions were selected on the micro characteristic section of the forming area to observe the change in thickness of the section. The test positions of the wall thickness of the forming area of the sample are shown in Fig. 4, the measurement result is the average of five samples, the measurement results of the wall thickness of the forming area are shown in Fig. 5. The thinning rate is calculated by the Eq. (1):

$$T(\%) = \frac{t_0 - t_i}{t_0} \times 100\%, 1,2,3 \ldots 7 \quad (1)$$

where t_0 is the initial thickness of the sample, and t_i is the thickness at the measurement position on the section of the formed microfeature.

The wall thickness of the cold-rolled material was 100 μm. Position 4 in Fig. 4 is the maximum thinning rate of the sample. The maximum thinning rate of the sample treated by pulse current-assisted laser shock treatment was 10.87%, the maximum thinning rate of laser shock treated sample was 23.61%, the average wall thickness of the LSF-treated sample was 86.7 μm, the average thinning rate was 13.3%, and the average wall thickness of the EP-LSF-treated sample was 93.4 μm. The average thinning rate was 6.6%. The results show that the thinning rate of the samples treated by pulsed current-assisted laser shock treatment decreased significantly.

3.2 Strain rate sensitivity coefficient

Tensile test is an effective method of testing the plasticity of materials. To study the effect of pulse current on the plasticity of materials, the tensile test was divided into two groups, namely, the cold-rolled state and 30-A pulse current treatment, and each group was set with five different levels of strain rates for stretching. The experimental results of the σ–ε curves of different strain rates are shown in Fig. 6. At the same stretching rate, the flow stress of the pulse current-treated samples was significantly lower than that of the untreated cold-rolled samples. The strain rate sensitivity coefficient refers to the sensitivity coefficient of the flow stress to the rate of change when the material is plastically deformed, that is, the parameter of the material strengthening tendency when the strain rate increases. In this study, the equal strain rate stretching method was adopted, and the stress values at the strains at 0.5, 0.75, 1, 1.25, and 1.5 mm were taken. A. Arieli [21] proposed that the strain rate sensitivity coefficient(m) can be obtained from the Eq. (2):

$$m = \frac{\partial \ln \sigma}{\partial \ln \varepsilon} \quad (2)$$

where σ is the true stress, ε is the true strain.

The test results are shown in Fig. 7. When the strain was 0.5 mm, the m of the pulse current treatment sample increased from 0.1140 to 0.1188, and that of the pulse current-treated sample increased from 0.1228 to 0.1348 when the strain was 0.75 mm. When the strain was 1 mm, M increased from 0.1117 to 0.1452. The results show that pulse current treatment can effectively improve the strain rate sensitivity coefficient of the material. Previous studies have shown that the stress concentration of the material can be effectively reduced by increasing the strain rate sensitivity coefficient, and the tendency of material necking under high strain rate loading can be reduced [22]. This phenomenon indicates that the material is more favorable for loading at a high strain rate (LSF) than that of cold rolling.

Ling et al. [23] prepared magnesium alloy using the extrusion method, studied the effect of strain rate on the strain rate sensitivity coefficient, and found that the strain rate sensitivity coefficient increases with the strain rate, proving that the strain rate sensitivity coefficient of the AZ31 magnesium alloy pretreated by laser shock pulse current can further improve the strain rate sensitivity coefficient to improve the formability of the material.

The laser shock free bulging experiment and strain rate sensitivity coefficient test results reveal that EP-LSF can effectively improve the micro-forming properties of magnesium alloys. To better reveal the EP-LSF mechanism that improves the micro-forming properties of magnesium alloys, Section 3.3 presents the study from three aspects, namely, grain size morphology, texture density, and microstructure evolution.

3.3 Microstructure characteristics

3.3.1 Grain size and morphology evolution

Grain size and morphology are closely related to the properties of materials and are two of the fundamental factors affecting the mechanical properties of mechanical materials. Therefore, studying the evolution of magnesium alloy grains during pulsed current-assisted laser shock is of great significance. Tan [24] found that the dynamic recrystallization temperature of AZ31 magnesium alloy in conventional forming was 250℃. The experiment in Section 2.2 shows that when the current parameter is 30 A and the sample temperature is approximately 250 ℃ , the sample can reach the required temperature for dynamic recrystallization.

The microstructures of the cold-rolled sample, the 25- and 30-A pulse current treatment sample, and the 30-A pulse current treatment sample after 40% laser energy shock treatment are shown in Fig. 8. Fig. 8(a) shows the microstructure of the cold-rolled sample. The rolled sample plate was produced by intense rolling, which produces a large plastic deformation, elongating the internal grains of the sample in the rolling direction, and forming elongated original grains and numerous deformation twins inside, which shows that the internal stress of the cold-rolled sample was relatively large and had obvious

anisotropy. Fig. 8(b) shows the sample treated with 25 A of pulse current. At this time, the temperature was 150 ℃, and most of the deformed area was beginning to disappear. Given the low current density, the Joule heat generated was insufficient to reach the temperature required for dynamic recrystallization, and the sample still exhibited elongated grains. This phenomenon shows that the plasticity of the sample has not been effectively improved. Fig. 8(c) shows the sample treated with 30 A of pulse current. At this time, the temperature was 250 °C, reaching the dynamic recrystallization temperature of the magnesium alloy. Many elongated grains parallel to the rolling direction in the sample had completely disappeared, and small and relatively uniform equiaxed grains appeared. The average grain size is approximately 6 μm. Fig. 8(d) shows the sample treated with 40% laser energy after 30-A pulse current treatment. The EP-LSF treated sample showed a high density of finer grains in the forming area Compared with the sample treated with pulse current. The grain was refined into a sub-grain structure.

Fig. 8 shows that when the pulse current was 30 A, the uniform and fine equiaxed grains in Fig. 8(c) completely replaced the elongated original grains in Fig. 8(a), indicating that pulse current can effectively reduce the initial grain size of the material. After LSF, high-density finer grains appeared in the sample forming area in Fig. 8(d), indicating that EP-LSF can further refine the grains after EPT refines the initial grains and improve the uniformity of the material. This phenomenon indicates that EP-LSF can improve the micro-forming properties of magnesium alloys by refining the grains further. Liu [25] proposed the grain refinement mechanism of pure titanium laser shock forming: (1) the onset of twins; (2) development of dislocation tangles (DTs) in the original grains and dislocation cells (DCs) formed by DTs; (3) evolution of DCs into sub-grains and high misoriented grains. Therefore, EP-LSF can also refine grains further through this mechanism.

3.3.2 Texture evolution

The orientation distribution of texture has a significant influence on the mechanical properties of materials. Thus, the texture evolution of materials after pulsed current-assisted laser shock must be studied. Fig. 9 shows the XRD patterns of AZ31 magnesium alloy after cold rolling and 30-A pulse current treatment. The α-Mg matrix and the β-$Mg_{17}Al_{12}$ phase are the main phases in the cold-rolled and pulse-current-treated samples. Nearly no other elements can be found in magnesium alloys. The diffraction pattern indicates that the crystal face of the cold-rolled sample (0001) had the strongest peak value, which was obtained by the strong rolling of the plate, which made the magnesium alloy produce a strong matrix texture in the rolling direction. Compared with the cold rolled sample, the diffraction peaks of the {0001} crystal plane of the sample treated by pulse current are obviously decreased; the {10-10}, {10-11}, and {10-12} crystal plane diffraction peaks decreased in varying degrees; and the {20-21} crystal plane diffraction peaks completely disappeared. However, the diffraction peak of the {10-13} crystal plane was enhanced, indicating that the grain orientation of magnesium alloy changed after pulse current treatment.

To further study the effect of pulsed current-assisted laser shock on the texture of magnesium alloys, Fig. 10 presents the pole diagrams with the {0001} and {10-10} crystal planes as the projection base. Fig. 10(a) shows the cold-rolled sample; the maximum pole density of the {0001} type texture is 23, and the maximum pole density of the {10-10} type texture is 3.4. Fig. 10(b) shows the 30-A pulse current treatment sample. The maximum pole density of the (0001) type texture is 15, and the maximum pole density of the {10-10} type texture is 2.9. Fig. 10 shows that the pulse current treatment reduced the maximum pole density of the sample (0001) type texture from 23 to 15, and the maximum pole density of the {10-10} type texture from 3.4 to 2.9.

Magnesium alloy rolled sheets have strong (0001) basal surface texture due to rolling. The extremely dense (0001) type texture is not conducive to the activity of basal < a > slips and can easily cause bending, cracks, and even fracture the material. The results in Fig. 10 show that pulse current treatment can reduce the initial texture density of the magnesium alloy (0001) and {10-10} type textures, indicating that the pulse current treatment enhances the activity of basal < a > slips by reducing the texture density. The activities improve the anisotropy [26], thereby improving the micro-forming properties of AZ31 magnesium alloy. Tiwaria et al. [17] used a SHTB to study the deformation behavior of an aluminum-zinc-magnesium-copper alloy at a high strain rate and found that the overall texture of the alloy weakened with the increase of the strain rate, indicating that high strain rate (LSF) can reduce the texture strength of the material. This proves that EP-LSF can improve the micro-formability of magnesium alloys by further weakening the strength of the texture.

3.3.3 Microstructure evolution

The evolution of microstructure also plays an important role in the formability of magnesium alloy. As the magnesium alloy foil is obtained by strong rolling, many dislocations accumulate in the material, resulting in high dislocation density in the cold-rolled sample, which seriously affects the micro formability of magnesium alloy. Many existing methods can be used to characterize the dislocation density. Gay et al. [27] studied the dislocation density of the material through the XRD data of different metals and found that when the dislocations are distributed in order, the dislocation density can be expressed by the following Eq. (3):

$$\rho = \frac{\beta}{|b|t\ \sqrt{2\pi \ln 2}} \qquad (3)$$

where ρ is the dislocation density, β is the half-maximum width, b is the Burgers Vector, and t is the single cell size.

Later, on the basis of his research, Dumn [28] found that when dislocations are randomly distributed, the relationship between dislocation density and full width at half maximum (FWHM) is as Eq. (4):

$$\rho = \frac{\beta^2}{2(\ln 2)\pi b^2} \approx \frac{\beta^2}{4.35 b^2}. \qquad (4)$$

Previous studies have shown that many inhomogeneous high-density dislocations are generated in magnesium alloy under the action of ultra-high strain rate laser shock wave, and the dislocation arrangement has no directionality [29]. Therefore, the relationship between the dislocation densities of EP-LSF and FWHM can be characterized by Eq. (4). According to the XRD patterns of the cold-rolled and pulse current treated samples measured in Fig. 7, the half width of cold-rolled samples is 0.211, while that of the 30-A pulse current treated samples is 0.104. According to Eq. (4), the dislocation density of cold-rolled magnesium alloy is significantly higher than that of the sample treated by pulse current, proving that pulse current can significantly improve the diffusion ability of the material, promote the dislocation annihilation of cold-rolled magnesium alloy, and improve the formability of magnesium alloy.

3.4 Corrosion Characteristics

3.4.1 SEM

Fig. 11 shows the surface morphology of the cold-rolled sample, the 80% laser energy impact sample, the 35-A pulse current treatment sample, and the 35-A pulse treatment sample after 80% laser energy impact in 3.5% NaCl solution corrosion. Fig. 11(a) shows that a large area of the corrosion exfoliation layer and large and dense corrosion pits appear on the surface of the cold-rolled samples. The surface of the sample has many corrosion cracks, which intersect, and the width and length of the cracks are large. The surface of the sample is seriously corroded. Fig. 11(c) shows that the magnesium alloy treated by pulse current has no large area of corrosion exfoliation layer and reduced area and number of corrosion pits and width and length of corrosion cracks. Figs. 11(b) and (d) show a large corrosion free area on the laser impact sample; the corrosion pit area decreased significantly, the corrosion cracks and corrosion holes disappeared, and the corrosion behavior of the sample surface was obviously inhibited. Compared with pulsed current-assisted laser shock treatment sample, the laser shock treated samples had few large area corrosion pits and numerous uniform corrosion spots. The corrosion morphology in Fig. 11(d) shows that the magnesium alloy subjected to pulsed current-assisted laser shock has the strongest corrosion resistance.

3.4.2 Polarization curves and EIS analysis

This study used polarization curves and EIS to characterize the effect of EP-LSF on the corrosion resistance of AZ31 magnesium alloys. The polarization curves of the cold-rolled, 35-A pulse current treatment, and 35-A pulse treatment of 80% laser energy shock samples are shown in Fig. 12. The cathodic polarization curve represents the hydrogen evolution at the cathode, and the anode polarization curve represents the dissolution of magnesium in the corrosive solution [30]. The corrosion potential of the cold-rolled sample is -1.425 V, and the corrosion current density is 5.226 μA/cm□. The corrosion potential of the EP-treated samples is moving toward -1.288 V, and the corrosion current density is reduced to 2.95 μA/cm□. The corrosion potential of the EP-LSF treated samples is moving toward -0.724 V, and the corrosion current density is reduced to 1.93 μA/cm□. Fig. 13 shows the

electrochemical impedance spectra of the cold-rolled, 35-A pulsed current treatment, and the 80% laser energy impact samples after the 35-A pulse treatment. Fig. 13 shows that the radius of the capacitance impedance loop and the electrochemical impedance value of the sample treated by pulse current increased compared with those of the cold-rolled sample, and the radius and electrochemical impedance value of the EP-LSF sample further increased compared with the sample treated by pulse current. The higher the corrosion potential was, the lower the corrosion current density and the higher the electrochemical impedance value were, indicating that the corrosion resistance of the material is better [31] the EP-LSF treated sample has the best corrosion resistance.

Wang et al. [32] proposed that high dislocation and twin density reduce the electrochemical potential of magnesium alloy, and stacking dislocation and high residual stress increase the local corrosion around the twins and accelerate the corrosion rate of magnesium alloy. Combined with the conclusion in Section 3.3.3, the comparison with the cold-rolled sample indicates that the dislocation density of the pulse current treatment sample decreased significantly, indicating that pulse current treatment can improve the corrosion resistance of magnesium alloy by reducing the dislocation density. Ralston et al. [33] proposed that the grain boundary density increases due to grain refinement, and the corrosion rate decreases with the grain size. Zhang et al. [34] found that the surface passivation rate of stainless steel can be effectively improved with an ultra-fine grain size. In Section 3.3.1, Figs. 8 (c) and (d) show that pulsed current-assisted laser shock can refine grains further, which also indicates that EP-LSF can improve the surface passivation rate of magnesium alloy by further refining the grains, thus improving the corrosion resistance of magnesium alloy.

Combined with the corrosion morphology and polarization curve of the sample surface, the EIS data indicate that pulse current pretreatment can improve the corrosion resistance of magnesium alloys, and pulse current-assisted laser shock strengthening can further improve the resistance of materials.

3.5 Inertial effect

The generation of cracks not only affects the forming ability of materials but also accelerates the corrosion rate of materials [35]. Relevant studies show that high strain rate can significantly improve the inertia effect of materials, and the inertia effect helps reduce the crack growth rate in the plastic deformation process [36–38]. Polese [39] found that laser shock can effectively inhibit the fatigue crack propagation of a 2024 aluminum alloy sheet. This phenomenon shows that LSF can improve the corrosion resistance of materials by suppressing the crack propagation speed. Kumar [40] found that the fatigue crack healing of steel specimens can be achieved by applying pulsed current, indicating that pulsed current can improve the corrosion resistance of materials by promoting the healing of microscopic cracks in materials.

Fig. 14 presents the corrosion principle diagram of AZ31 magnesium alloy in 3.5% NaCl solution. Fig. 14(a) shows the EP-LSF-treated sample. Given the good forming quality of the

sample, a dense grain refinement layer formed on the surface of the material, which can effectively reduce the corrosion rate. Fig. 14(b) shows the LSF-treated sample. Given the poor forming ability of the cold-rolled magnesium alloy, the sample is prone to cracks during plastic deformation. Part of the α-Mg matrix was exposed to the corrosive solution, accelerating the corrosion of the material. This phenomenon indicates that EP-LSF can improve the formability and corrosion resistance of the material by delaying the crack growth during plastic deformation and promoting the healing of micro cracks.

Conclusions

In this study, a new material forming method, namely, EP-LSF, was used to study its effect on the micro formability and corrosion resistance of materials. The main results are summarized as follows:

1. Pulse current treatment significantly improves the strain rate sensitivity coefficient of the material. When the strain is 0.5mm, the value of m is increased to 0.1188, the strain is 0.75mm, and the value of m is increased to 0.1348, when the strain is 1mm, the value of m is increased to 0.1452.
2. After pulse current treatment, the original long grain of the material is refined into equiaxed grain. After laser shock, the grain in the forming area of the material is further refined, which indicates that EP-LSF treatment improves the micro formability of the material by further refining the grain.
3. Pulse current treatment reduces the texture density of the material, the maximum pole density of (0001) type texture is reduced to 15, and the maximum pole density of {10-10} type texture is reduced to 2.9. The reduction of the texture density of the material improves the micro-forming performance of the material during laser shock forming.
4. Pulse current can improve the corrosion resistance of cold-rolled magnesium alloy by reducing the dislocation density, and pulse current-assisted laser shock can further improve the corrosion resistance of magnesium alloy by refining the grain size.
5. Pulse current-assisted laser shock can improve the formability and corrosion resistance of the materials by delaying the crack growth during plastic deformation and promoting the healing of micro cracks.

Declarations

Ethical approval

Not applicable

Consent to participate

Not applicable

Consent to publish

Not applicable

Authors' contributions

Yuhao Sun wrote the first draft of the paper. All authors revised and approved the final version of the manuscript.

Funding

This work is supported by the National Natural Science Foundation of China (Grant No. 51675243).

Competing interests

The authors declare that they have no competing interests.

Availability of data and materials

Not applicable

References

[1] M. Kleiner, M. Geiger, A. Klaus (2003) Manufacturing of Lightweight Components by Metal Forming, Cirp. Ann-Manuf. Techn. 52: 521-542.

[2] X.P. Li, G.Y. Tang, J. Kuang, X.H. Li, J. Zhu (2014) Effect of current frequency on the mechanical properties, microstructure and texture evolution in AZ31 magnesium alloy strips during electroplastic rolling, Mater. Sci. Eng. A. 612: 406–413.

[3] I. Ulacia, C.P. Salisbury, I. Hurtado, M.J. Worswick (2011) Tensile characterization and constitutive modeling of AZ31 magnesium alloy sheet over wide range of strain rates and temperatures, J. Mater. Process. TECH. 211: 830–839.

[4] Q. Ma, H. El Kadiri, A.L. Oppedal, J.C. Baird,B. Li, M.F. Horstemeyer,S.C. Vogel (2012) Twinning effects in a rod-textured AM30 Magnesium alloy, Int. J. Plasticity. 29: 60-76.

[5] W.Q. Zhou, D.Y. Shan, E.H. Han, W. Ke (2008) Structure and formation mechanism of phosphate conversion coating on die-cast AZ91D magnesium alloy, Corros. Sci. 50: 329–337.

[6] Y.F. Tang, L.X. Zhu, P. Zhang, K. Zhao, Z.X. Wu (2020) Enhanced corrosion resistance of bio-piezoelectric composite coatings on medical magnesium alloys, Corros. Sci. 176: 108939.

[7] B. Nagarajan, S. Castagne, Z.K. Wang (2013) Mold-free fabrication of 3D microfeatures using laser-induced shock pressure, Appl. Surf. Sci. 268: 529-534.

[8] Y.X. Ye, T. Xuan, Z.C. Lian, X.J. Hua, Y.H. Fu (2015) Fabricating micro embossments on the metal surface through spatially modulating laser-induced shock wave, Appl. Surf. Sci. 357: 678-688.

[9] C. Zheng, Z.R. Tian, X.H. Zhao, Y.C. Tan, G.F. Zhang, G.Q. Zhao (2020) Effect of pulsed laser parameters on deformation inhomogeneity in laser shock incremental forming of pure copper foil, Opt. Laser. Technol. 127: 106205.

[10] K. Liu, X.H. Dong, H.Y. Xie, F. Peng (2015) Effect of pulsed current on the deformation behavior of AZ31 magnesium alloy, Mater. Sci. Eng. A. 623: 97-103.

[11] F. Feng, S.Y. Huang, Z.H. Meng, J.H. Hu, Y. Lei, M.C. Zhou, D. Wu, Z.Z. Yang (2014) Experimental study on tensile property of AZ31 magnesium alloy at different high strain rates and temperatures, Mater. Design. 57: 10-20.

[12] R.B. Raj Kumar, M.Y. Ismail, V.S. Vijayarasi, V.S. Senthil Kumar (2020) Effect of grain refinement on superplastic forming of magnesium alloy AZ31 under three different conditions using rectangular die. Materialstoday: Proceedings. 22: 364-369.

[13] S. Hui, Z.J. Wang (2011) Grain refinement by means of phase transformation and recrystallization induced by electro-pulsing, Trans. Nonferrous Met. Soc. China. 21: 353-357.

[14] X. Xu, J. Zhang, H.G. Liu, Y. He, W.H. Zhao (2019) Grain refinement mechanism under high strain-rate deformation in machined surface during highspeed machining Ti6Al4V, Mater. Sci. Eng. A. 752: 167-179.

[15] H. Zhang, Z.C. Ren, J. Liu, J.Y. Zhao, Z.K. Liu, D. Lin, R.X. Zhang, M. J. Graber, N.K. Thomas, Z.D. Kerek, G.X. Wang, Y.L. Dong, C. Ye (2019) Microstructure evolution and electroplasticity in Ti64 subjected to electropulsing-assisted laser shock peening, J. Alloys Compd. 802: 573-582.

[16] Y.B. Jiang, G.Y. Tang, C.H. Shek, W. Liu (2011) Microstructure and texture evolution of the cold-rolled AZ91 magnesium alloy strip under electropulsing treatment, J. Alloys Compd. 509: 4308-4313.

[17] S. Tiwari, S. Mishra, A. Odeshi, J.A. Szpunar, M. Chopkar (2017) Evolution of texture and microstructure during high strain rate torsion of aluminium zinc magnesium copper alloy, Mater. Sci. Eng. A. 683: 97-102.

[18] Y.R. Liu, K.M. Zhang, J.X. Zou, D.K. Liu, T.C. Zhang (2018) Effect of the high current pulsed electron beam treatment on the surface microstructure and corrosion resistance of a Mg-4Sm alloy, J. Alloys Compd. 741: 65-75.

[19] M. Abeens, R. Muruganandhan, K. Thirumavalavan (2020) Effect of Low energy laser shock peening on plastic deformation wettability and corrosion resistance of aluminum alloy 7075 T651, Optik. 219 165045.

[20] V.K. Caralapatti, S. Narayanswamy (2017) Effect of high repetition laser shock peening on biocompatibility and corrosion resistance of magnesium, Opt. Laser. Technol. 88: 75-84.

[21] A. Arieli, A. Rosen (1976) Measurements of the strain rate sensitivity coefficient in superplastic Ti–6Al--4V alloy, Scripta. Mater. 10: 471-475.

[22] M.Y. Li, A. Chandra (1999) Influence of strain-rate sensitivity on necking and instability in sheet metal forming, J. Mater. Process. Tech. 96: 133–138.

[23] L.B. Ren, M.Y. Zhou, T.H. Lu, L.L. Fan, Y.Y. Guo (2020) Y.W. Zhang, C.J. Boehlert, G.F. Quan, Eutectic phase strengthening and strain rate sensitivity behavior of AZ80 magnesium alloy, Mater. Sci. Eng. A. 770: 138548

[24] J.C. Tan, M.J. Tan (2003) Dynamic continuous recrystallization characteristics in two stage deformation of Mg-3A-1Zn alloy sheet, Mater. Sci. Eng. A. 339: 124-132.

[25] H.X. Liu, Y. H u, X. Wang, Z.B. Shen, P. Li, C.X. Gu, H. Liu, D.Z. Du, C. Guo (2013) Grain refinement progress of pure titanium during laser shock forming (LSF) and mechanical property characterizations with nanoindentation, Mater. Sci. Eng. A. 564: 13-21.

[26] L.F. Wang, Y.Q. Li, H. Zhang, Z.Y. Zhang, Q.S. Yang, Q. Zhang, H.X. Wang, W.L. Cheng, K.S. Shin, M. Vedani (2020) Review: Achieving enhanced plasticity of magnesium alloys below recrystallization temperature through various texture control methods, J. Mater. Res. Technol. 9: 12604 -12625.

[27] P.Gay, P.B. Hirsch, A. Kelly† (1953) The estimation of dislocation densities in metals from X-ray data, Acta. Mater. 1: 315-319.

[28] C.G. Dunn, E.F. Kogh (1957) Comparison of dislocation densities of primary and secondary recrystallization grains of Si-Fe, Acta. Mater. 5: 548-554.

[29] U. Trdan, M. Skarba, J. Grum (2014) Laser shock peening effect on the dislocation transitions and grain refinement of Al–Mg–Si alloy, Mater. Charact. 97: 57-68.

[30] Y. Shadangi, K. Chattopadhyay, S.B. Rai, V. Singh (2015) Effect of LASER shock peening on microstructure, mechanical properties and corrosion behavior of interstitial free steel, Surf. Coat. Tech. 280: 216–224.

[31] U. Trdan, J. Grum (2012) Evaluation of corrosion resistance of AA6082-T651 aluminium alloy after laser shock peening by means of cyclic polarisation and EIS methods, Corros. Sci. 59: 324-333.

[32] W.H. Wang, H.L. Wu, R. Zan, Y. Sun, C.Blawert, S.X. Zhang, J.H. Ni, M.L. Zheludkevich, X.N. Zhang (2020) Microstructure controls the corrosion behavior of a lean biodegradable Mg–2Zn alloy , Acta. Biomater. 107: 349–361.

[33] K.D. Ralston, D. Fabijanic, N. Birbilis (2011) Effect of grain size on corrosion of high purity aluminium, Electrochim. Acta. 56: 1729–1736.

[34] H. Zhang, P. Xue, Q.N. Song, D. Wang, B.L. Xiao, Z.Y. Ma (2020) Effect of grain ultra-refinement on corrosion behavior of ultra-high strength high nitrogen stainless steel, Corros. Sci. 174: 108847.

[35] Y.W. Hao, B. Deng, C. Zhong, Y.M. Jiang, J. Li (2009) Effect of Surface Mechanical Attrition Treatment on Corrosion Behavior of 316 Stainless Steel, J. Iron. Steel. Res. Int. 16: 68-72.

[36] L. Ren, X.M. Yu, Y. He, K. Wang, H.L. Yao (2020) Numerical investigation of lateral inertia effect in dynamic impact testing of UHPC using a Split-Hopkinson pressure bar, Conster. Build. Mater. 246: 118483.

[37] N. Jacques, S. Mercier, A. Molinari (2012) Effects of microscale inertia on dynamic ductile crack growth, J. Mech. Phys. Solids. 60: 665-690.

[38] C.Z. Qi, C. Xia, X.Z. Li, Y.J. Sun (2019) Effect of inertia and crack propagation on dynamic strength of geologic-type materials, Int. J. Impact. Eng. 133: 103367.

[39] D.C.V. Aswegen, C. Polese (2021) Experimental and analytical investigation of the effects of laser shock peening processing strategy on fatigue crack growth in thin 2024 aluminium alloy panels, Int. J. Fatigue. 142: 105969.

[40] A. Kumar, S.K. Paul (2020) Healing of fatigue crack in steel with the application of pulsed electric current, Materialia. 14: 100906.

Figures

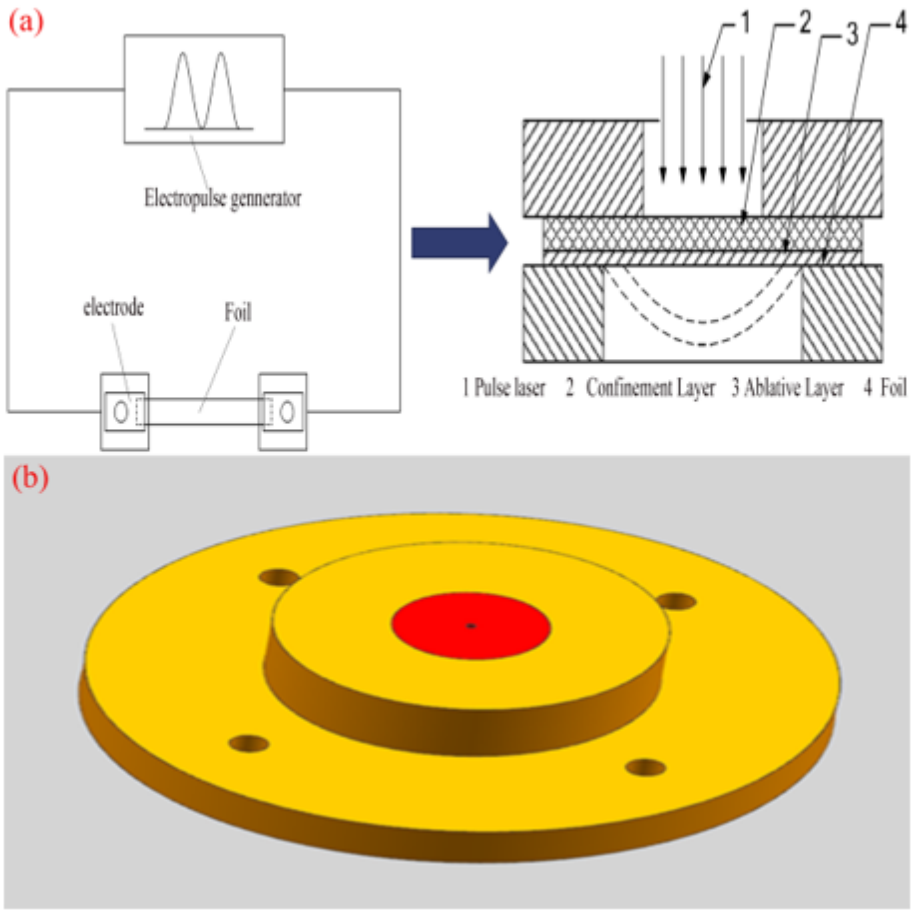

Figure 1

(a) experimental schematics of EP-LSF, (b) die diagram of EP-LSF.

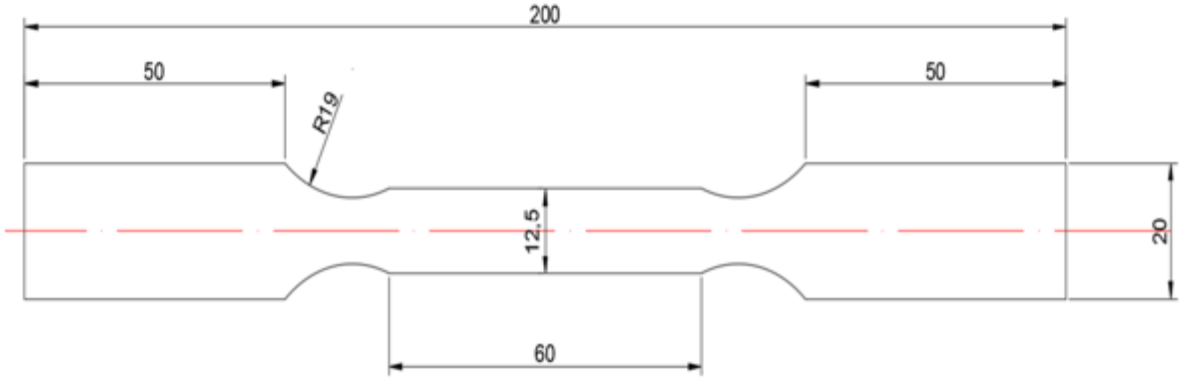

Figure 2

Dimensions of AZ31 uniaxial tensile specimen.

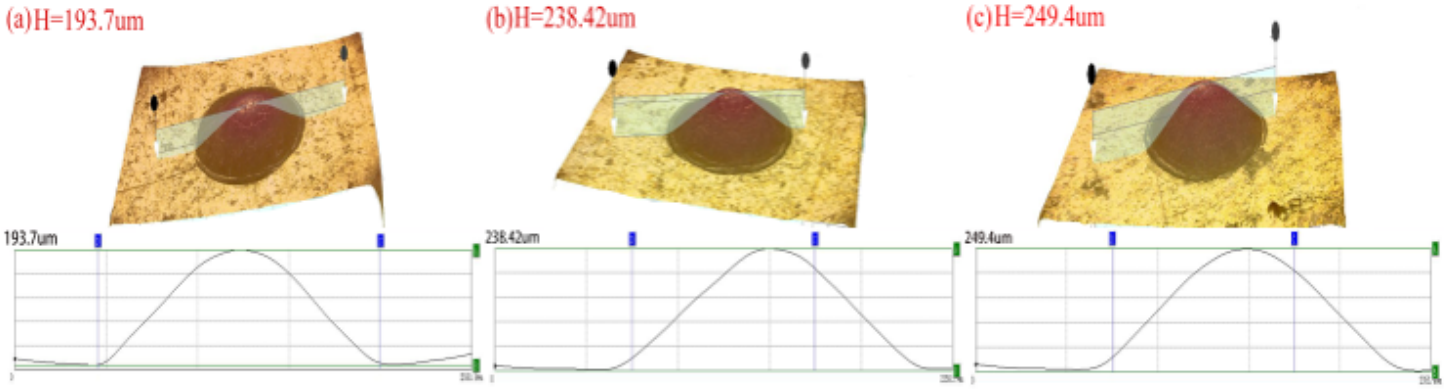

Figure 3

Diagram of forming height (a) 0 A, (b) 25 A, (c) 30 A.

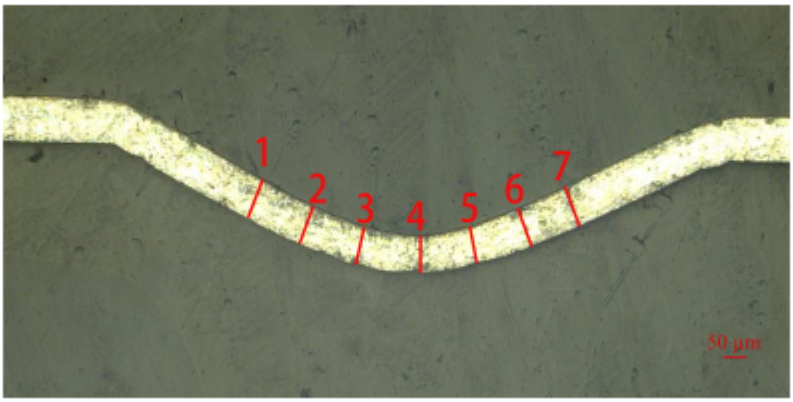

Figure 4

Test position of wall thickness in forming area.

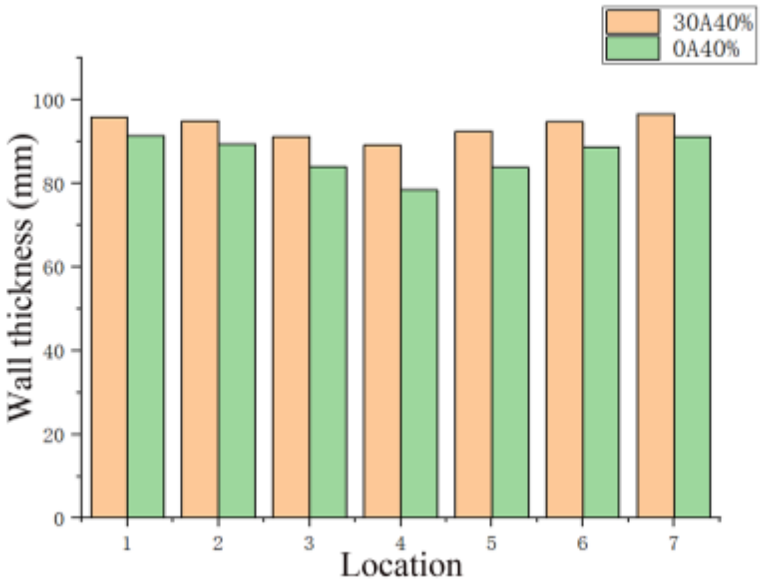

Figure 5

Measurement results of section thickness in forming area.

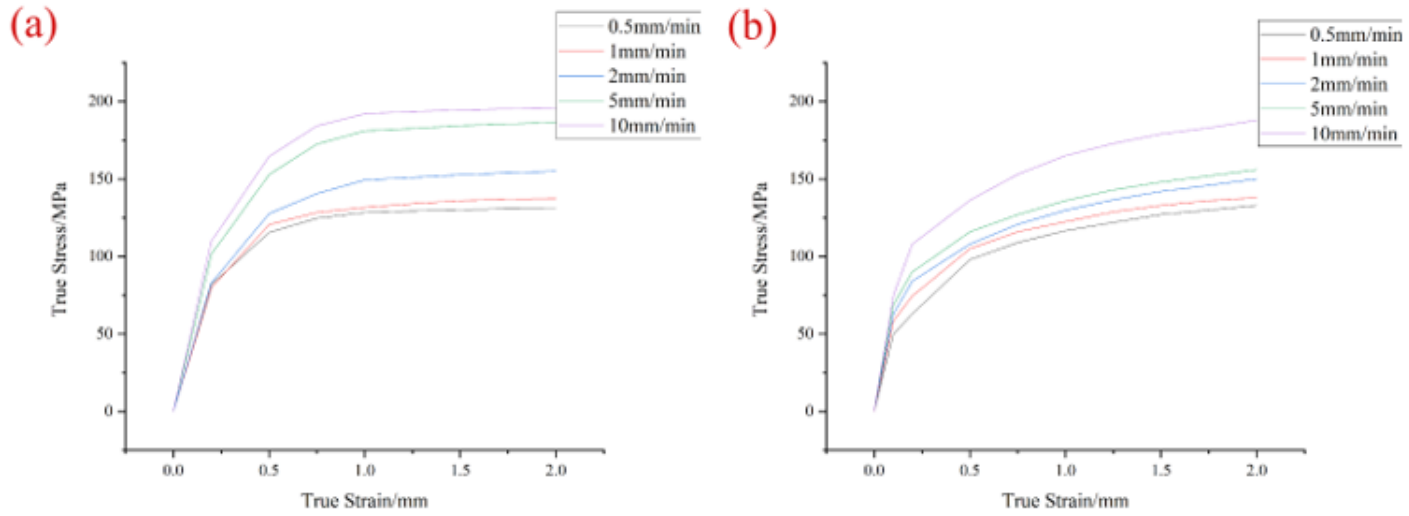

Figure 6

Stress-strain curves (a) 0 A, (b) 30 A.

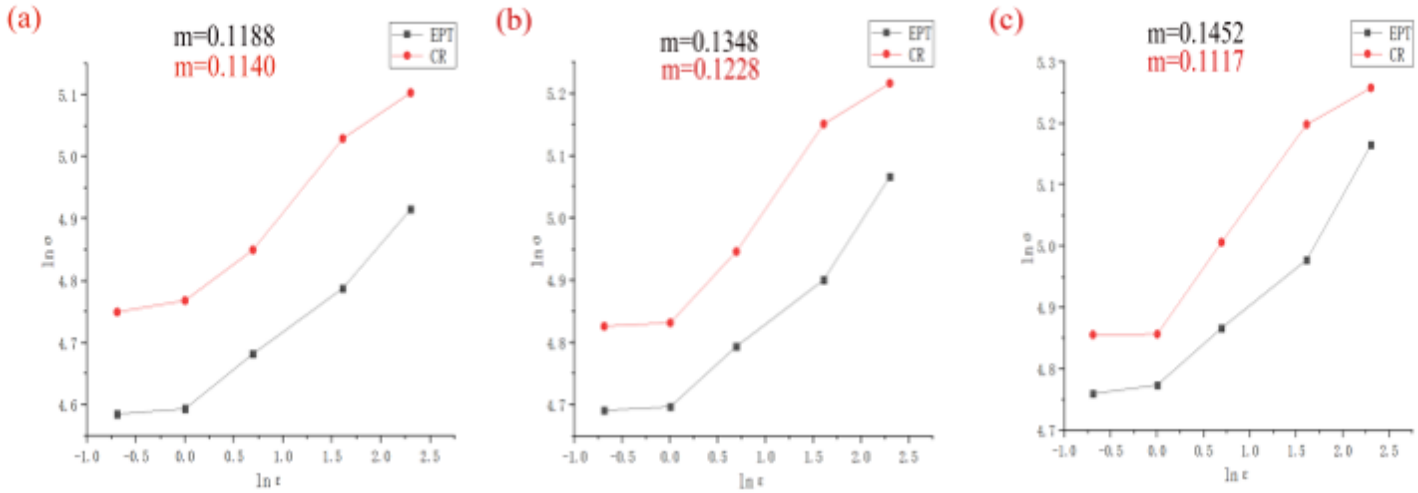

Figure 7

Strain rate sensitivity coefficient of different strains (a) strain 0.5 mm, (b) strain 0.75 mm, (c) strain 1mm.

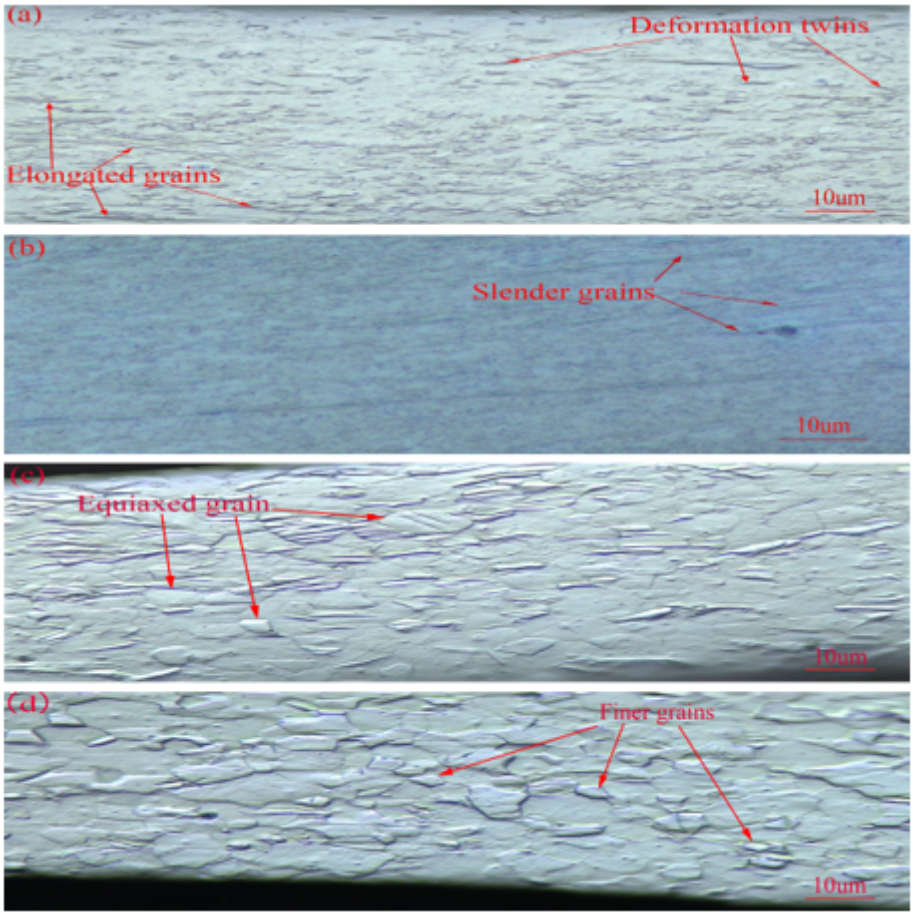

Figure 8

Grain size and morphology (a) 0 A, (b) 25 A, (c) 30 A, (d) 30 A40%.

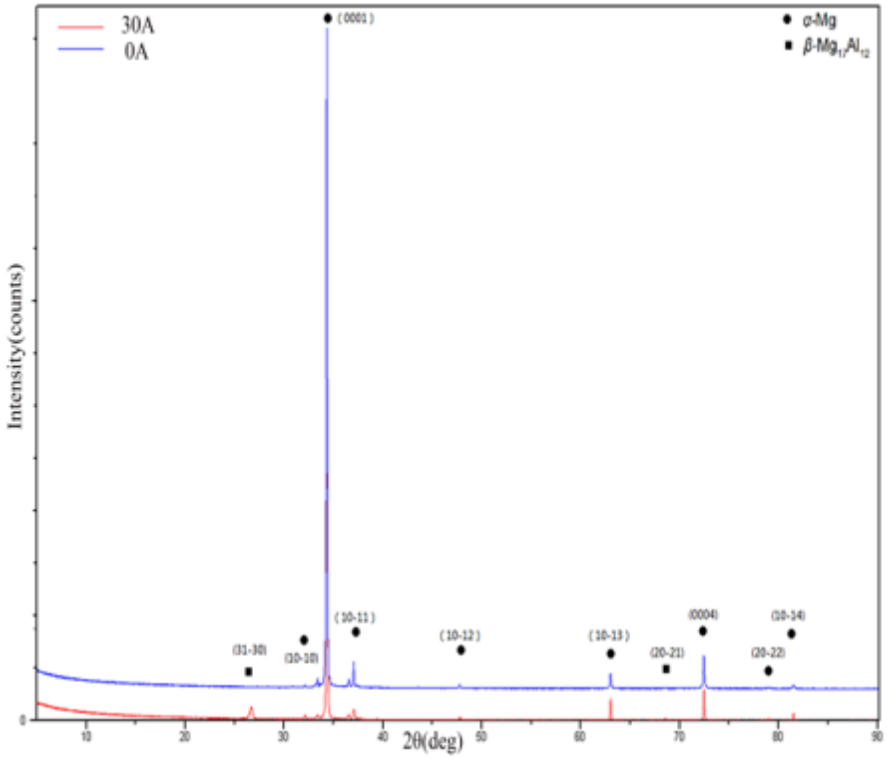

Figure 9

X-ray diffraction pattern.

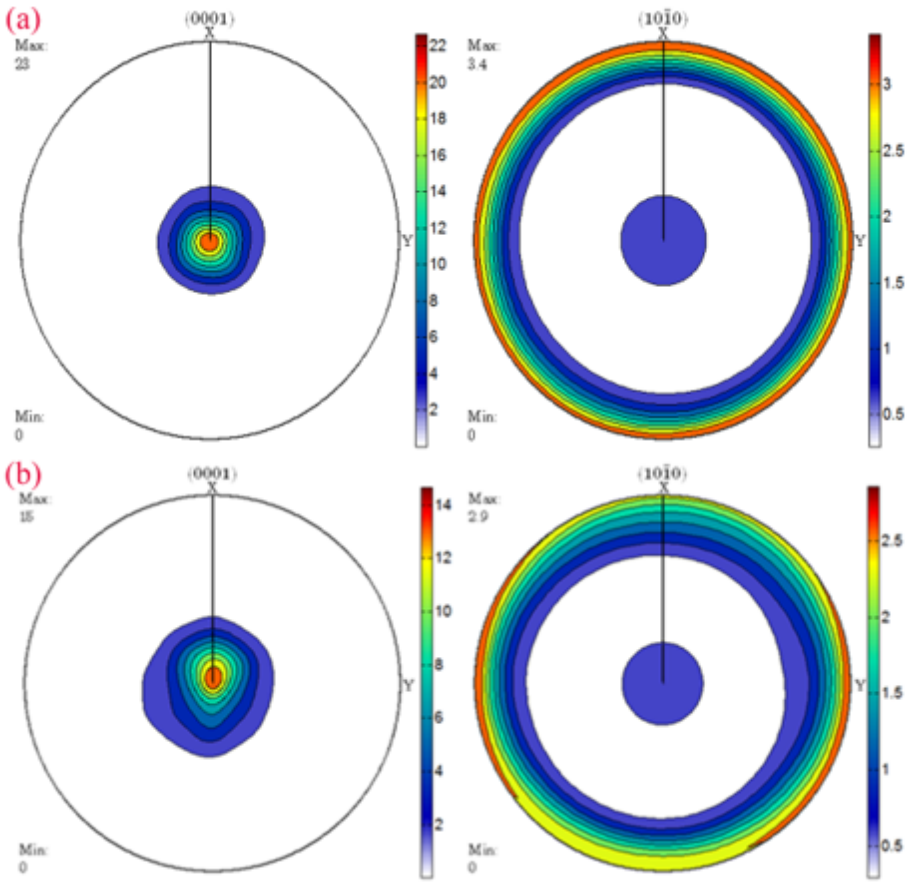

Figure 10

Pole figures (a) Cold rolled, (b) 30 A.

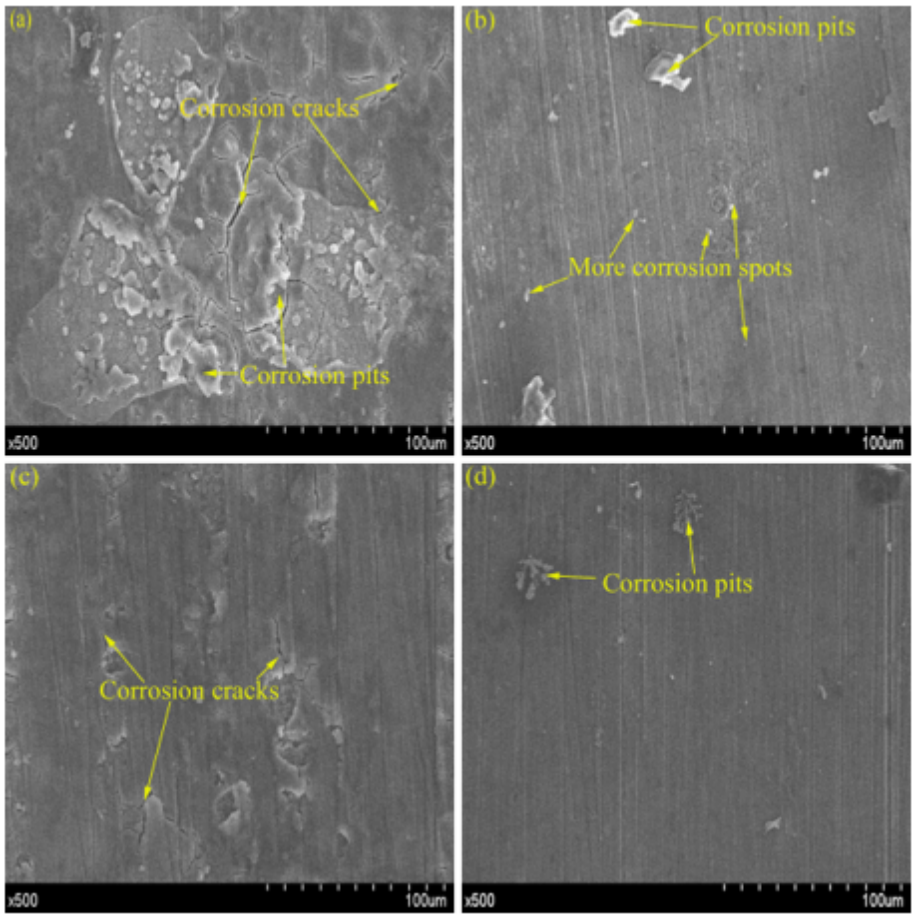

Figure 11

SEM images of corrosion samples (a) cold rolling, (b) 0 A80%, (c) 35 A, (d) 35 A80%.

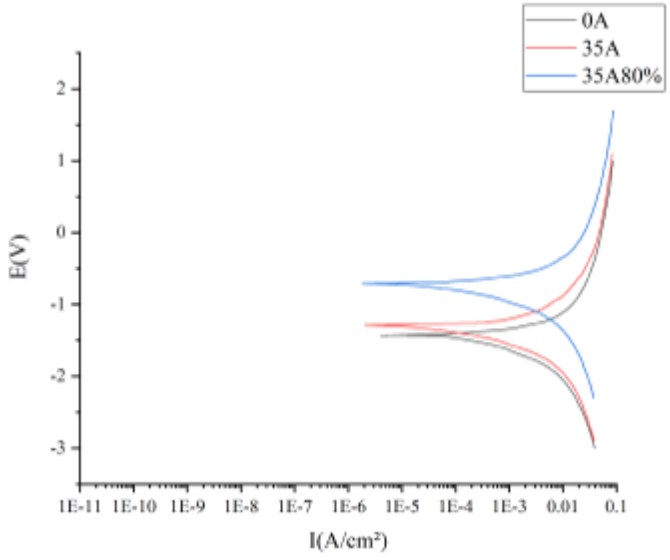

Figure 12

Polarization curves of cold rolled, 35A and 35A80% samples in 3.5% NaCl solution.

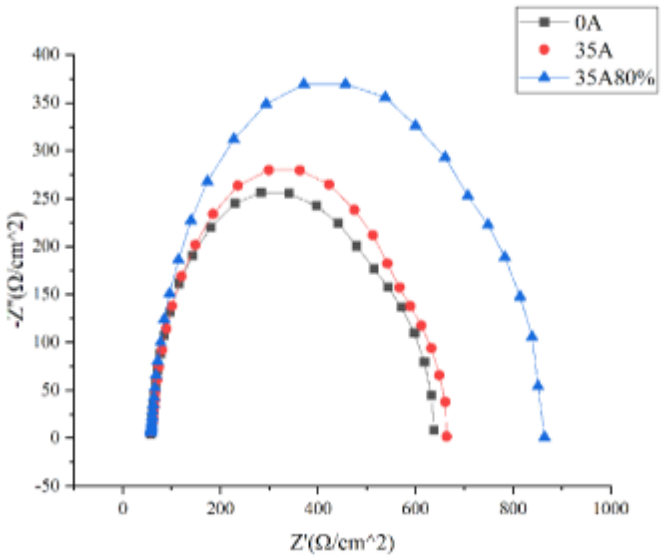

Figure 13

Nyquist plot of cold rolled, 35A and 35A80% samples in 3.5% NaCl solution.

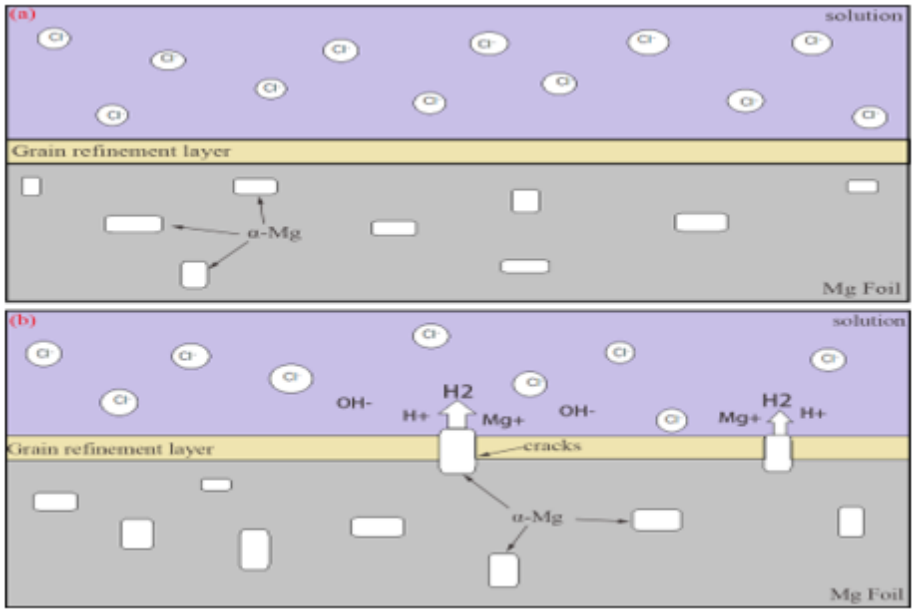

Figure 14

corrosion schematic diagram of sample in 3.5% NaCl solution (a) EP-LSF treated sample, (b) LSF treated sample.